Experimental Study of Liquid Spray Mode of Twin Fluid Atomizer Using Optical Diagnostic Tool

Raju Murugan[1] · Saravanan Balusamy[1] · Pankaj Kolhe[1]

Abstract

Twin fluid atomizers allow for two different spray forming modes, flow focusing and flow blurring, depending on the operating, geometric, and thermophysical properties of the working liquids. In flow focusing mode, the liquid jet breaks outside the injector, whereas in flow blurring mode, the liquid jet breaks inside the atomizer. Operating conditions are believed to play an essential role in determining the size and velocity of droplets with specific geometric and fluid properties. This work investigates the effect of air flow rate and liquid flow rate on spray characteristics by varying them independently. The geometric parameters, height ($H = 0.3$ mm) and orifice diameter ($D = 1.5$ mm) of the atomizer are kept constant (with $H/D = 0.2$). Spray mode is identified using high-speed images. Phase Doppler particle analyzer is used to measure droplet size and velocity simultaneously. Regardless of liquid flow rate, flow focusing mode is observed at low air flow rate and flow blurring mode is observed at high air flow rate. In general, flow blurring mode produced smaller droplets at higher velocities than flow focusing mode. The Joint probability distribution function of droplet size and velocity shows unimodal near the exit of the atomizer and bimodal distribution around 50 mm downstream due to the completion of the secondary breakup around that position and the subsequent loss of momentum due to the resistance of the surrounding air from the injector outlet. Flow focusing mode showed that sauter mean diameter and mass median diameter tend to increase initially due to coalescence of the spray and begin to decrease due to secondary breakup. The joint probability distribution of droplet Weber number and the droplet Reynolds number indicate that the flow blurring spray produced finer and faster droplets than the flow focusing spray. Overlapping of two Gaussians representing smaller and larger droplets best fits the droplet probability distribution as compared to lognormal or gamma or beta distribution.

Abbreviations
AFR   Air flow rate

✉ Pankaj Kolhe
   psk@mae.iith.ac.in

[1]   Department of Mechanical and Aerospace Engineering, Indian Institute of Technology Hyderabad, Kandi, Sangareddy, Telangana State 502285, India

ALR	Air to liquid ratio
CDF	Cumulative distribution function
FB	Flow Blurring
FF	Flow Focusing
JPDF	Joint probability distribution function
LFR	Liquid flow rate
MMD	Mass median diameter
PDF	Probability distribution function
PDPA	Phase Doppler particle analyser
RSF	Relative Span Factor
SMD	Sauter mean diameter

1 Introduction

Sprays play an essential role in many areas, such as agricultural sprays, liquid fuel combustion, spray cleaning, spray painting, spray cooling, and spray dryers. The spray is a type of multiphase flow that is a collection of dynamically dispersed droplets in gas at various droplet sizes and velocity ranges. The process of creating a spray is called atomization, where the kinetic energy of a liquid or exposure to high-velocity air, liquid jet or sheet is broken down into multiple droplets. Spray characteristics such as spray cone angle, droplet size, droplet velocity, spray pattern, droplet size distribution, etc. play an essential role in liquid fuel combustion systems such as rocket engine, gas turbine engine, ramjet engine (subsonic and supersonic combustion), internal combustion engine, etc. In general, before burning, liquid fuels need to be dispersed in small droplets that are rapidly vaporized and mixed with the oxidizer. The atomization process increases the surface area of the fuel, increases the contact area between the fuel and the oxidizer, and improves mixing and combustion (Lefebvre 1989). Energy density content of liquid fuels have continued interests from various investigators (Kasabov et al. 2013; Stiehl et al. 2013; Wright et al. 2010; Bottone et al. 2012; Bhagwan et al. 2014) to find ways in improving liquid fuel combustion and emissions, and understanding of the spray development plays a huge role in it.

The performance and spray characteristics of the atomizer depend on the shape of the atomizer, operating parameters, and the physical properties of the dispersed and continuous phases. Typically, the atomization process involves two steps: primary atomization and secondary atomization. In primary atomization, the liquid jet breaks down into ligaments and large droplets. In secondary atomization, these ligaments/droplets are further divided into sub-droplets (Lefebvre 1989). The atomizer mainly consists of two types, namely (1) single fluid or pressure atomizer; it discharges the liquid at high-velocity by pressurizing the liquid through a fine orifice and (2) twin fluid atomizer (pneumatic or airblast), it exposes the relatively slow-moving liquid to a high-velocity air stream. Airblast atomizers have many advantages over pressure atomizers, especially in gas turbine engine applications (Lefebvre 1980).

Based on the mixing, twin fluid atomizers are divided into internal and external mixing atomizers. In internal mixing atomizer (Lorenzetto and Lefebvre 1977; Sovani et al. 2001; Lal et al. 2010; Liu et al. 2010; Ochowiak et al. 2010; Ma et al. 2013; Ochowiak 2013, 2016; Sun et al. 2018; Chen et al. 2018), liquid and gas mix in the injector (effervescent atomizer and air blast atomizer), whereas in the external mixing atomizer, liquid and gas mix outside of the injector (Marmottant and Villermaux 2004; Lujaji et al. 2016). When

compared to the same operating parameters, the spray characteristics of the internal mixing atomizer are different from those of the external mixing atomizer. This is because the primary atomization takes place in the injector and the spray is enhanced. Spray velocity is an important parameter in many spray applications. Liquid fuel combustion is one such application. In an internal mixing atomizer, the spray velocity depends on internal turbulent mixing. Nukiyama and Tanasawa (1938) performed various experiments using airblast atomizers to test various geometric, operating, and thermo-physical properties of the fluid. The results show that the effect of nozzle geometry plays an important role in atomization performance. For all types of nozzles, increasing the air velocity reduces the droplet size.

Gañán-Calvo (2005) has found that both internal and external mixing is possible, based on flow blurring atomization, where geometry plays an important role. In a flow-blurring twin fluid atomizer, the air flows perpendicular to the liquid flow upstream of the injector dump plane. Gañán-Calvo proposes to maintain H≤0.25D for flow blurring, H>0.25D for flow focusing. 'H' is the gap between the orifice and liquid tube end, and D is the diameter of the tube. Internal mixing is created by the divergence of high-velocity airflow in a liquid tube, leading to turbulent mixing of the two fluids, resulting in a better spray. This configuration is commonly known as a flow blurring (FB) configuration, as shown in Fig. 1. Recently, Murugan et al. (2018) conducted a systematic experimental study of different values H/D and air to liquid ratios (ALR) using a transparent two-fluid atomizer and schematics based on the inferences is shown in Fig. 1. Flow focusing behavior was observed even at low H/D = 0.05 and low ALR values. It may be noted in FF mode liquid jet is focused resulting in smaller jet spread than the exit orifice diameter. They found that with large amounts of ALR, FB could be achieved even at a higher H/D = 0.42. Based on these experimental studies, spray formation in FB mode depends on geometric H/D and
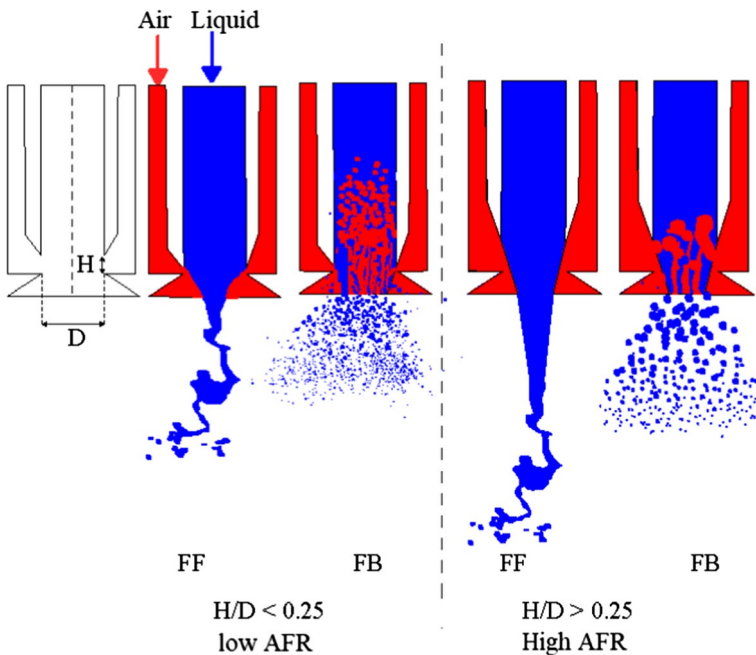

Fig. 1 Two different modes of spray formation: flow focusing (FF) and flow blurring (FB) for different (H/D) ratios (Murugan et al. 2018)

operating parameters ALR. It may be noted that FF and FB configuration mode of operation of pneumatic injector configuration (refer Fig. 1) can be predicted based on observation of the core jet like structure with flapping instability and focused jet with a smaller diameter than orifice exit. FF mode of operation shows the spray formation very similar to coaxial jets.

Atomizer performance is usually described by the mean droplet size produced under various operating conditions. Of these, the Sauter mean diameter is generally considered to be the most appropriate, as it is most relevant to the rate of evaporation and combustion. Mass median diameter is widely used in many applications, which is the drop diameter corresponding to 50% of the cumulative mass distribution curve (Lefebvre 1980). The joint probability distribution function (JPDF) is a multivariate generalization of the probability density function that characterizes the distribution of a continuous random variable. JPDF is useful in many engineering applications (Jensen and Guo 2017). Previous researchers used these variables to use JPDF for spray applications based on simultaneous multivariable measurements such as droplet velocity, droplet size, dimensionless numbers, etc. (Ayres et al. 2001; Jiang et al. 2016; Biswal et al. 2019; Panchasara et al. 2019).

Simmons et al. (2009) investigated air blast and flow blurring atomizer under the same operating conditions. The results showed that the FB atomizer produced smaller droplets than the air blast atomizer. The Azevedo et al. (2013a, b, 2016) has performed various experimental studies using a flow blurring atomizer on three different configurations of the injector outlet using different liquids. They showed that increasing ALR reduced SMD in all liquids. Jiang and Agrawal (2015a, b) conducted an experimental study of ALR = 2 using an FB atomizer for water and glycerol. Near-field PIV and high-speed imaging were performed on these two fluids. They showed that primary breakup occurred in the FB atomizer and atomization efficiency was improved. Fisher et al. (2017) have conducted experimental studies on various liquids with ALR = 3. Due to its low viscosity, water has been shown to produce small droplets compared to glycerol. Recently, Khan et al. (2019) performed various low liquid flow rate experiments using a flow blurring atomizer. They measured the diameter of the droplet using a shadowgraph imaging technique. They showed that when the LFR was reduced from 41.7 to 2.78 mg/s, the droplet size was reduced from 450 microns to about 30 microns.

The literature shows that most of the experimental investigations performed on twin fluid atomizers focused on the effect of ALR on spray behavior. However, the same ALR can be achieved by changing the AFR and LFR independently, and the individual effects on spray characteristics are unknown. Besides, from a practical application perspective, the turndown ratio is important and particularly at low flow rates, the pneumatic atomizer changes the mode of operation (refer Fig. 1). In the present study the operating parameter, atomizing air flow rate, is varied between Mach number of 0.2 to 0.48 based on bulk mean velocity estimation to understand the lower limit from spray quality perspective. Most of the reported works also studied behavior by measuring only droplet size or velocity. However, the simultaneous measurement of droplet size and velocity helps to better understand the basic characteristics of sprays under various operating conditions using JPDF of the dimensionless numbers.

Turndown ratio or the operation of combustor at lower firing rate is important from the poor emissions perspective, which could be attributed to the spray quality deterioration at low operating flow rates leading to larger droplets burning in the diffusion mode. Present study focusses on the spray quality for the pneumatic injector configuration considered (refer Fig. 1), and at low flow rates the mode of operation may change from FB to FF significantly deteriorating the spray quality. It may be noted that flow

blurring mode would always be observed at higher air flow rate compared to flow focussing mode of operation. In twin fluid atomizers, source of energy comes from atomizing air flow rate as the kinetic energy of air would be dissipated as surface energy creating a multiplicity of droplets. The objective of this study is to investigate the effect of operating parameters on the performance of a twin-fluid atomizer with specific geometric and physical properties of the fluid. Air and water are working fluids. High-speed images are used to identify spray modes under various operating conditions. PDPA technique measured droplet size and velocity simultaneously. The effect of AFR and LFR on the spray characteristics is investigated by varying them independently.

2 Experimental Method

2.1 Atomizer Unit

A twin fluid atomizer is designed and fabricated to study the spray behavior under various operating conditions similar to the industrial gas turbines. The atomizer is made of brass. The cross section of the atomizer is shown in Fig. 2. The atomizer unit mainly consists of three parts: injector body, spacer and injector cap. The injector body has separate passages for both liquid and air, which are shown as blue and red color in Fig. 2. The height of the spacer keeps exactly the required gap between the injector body and cap, as indicated by parameter H in Fig. 1. The injector cap has a central hole acting as an orifice. The diameter of the hole is indicated by the parameter D in Fig. 1. The H/D ratio can be varied by using different combinations of spacers. In this study, the H/D is kept constant at 0.2. D is kept at 1.5 mm and H at 0.3 mm.

The setup of the atomizer unit is shown in Fig. 3. Air mass flow is regulated using a mass flow controller (MCR 50 slpm, Alicat Scientific Inc.) with $\pm 0.8\%$ uncertainty in full-scale readings. Water from a 3-liter tank is supplied to the atomizer by a peristaltic pump, which regulates the flow rate with an uncertainty of $\pm 1.5\%$ of full-scale readings. A pulse dampener is used to reduce the pulsation from the peristaltic pump. Experiments were conducted at room temperature of about 298 K.
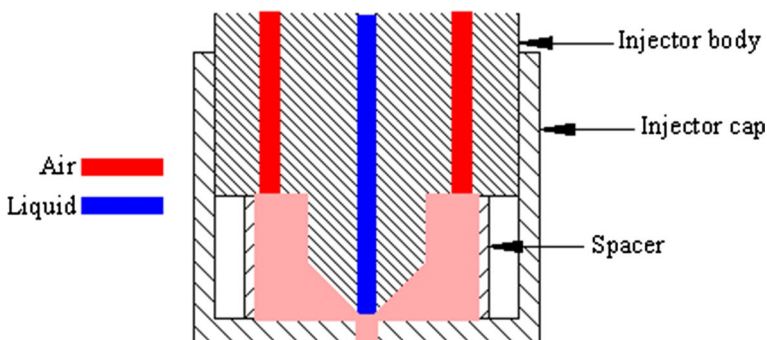

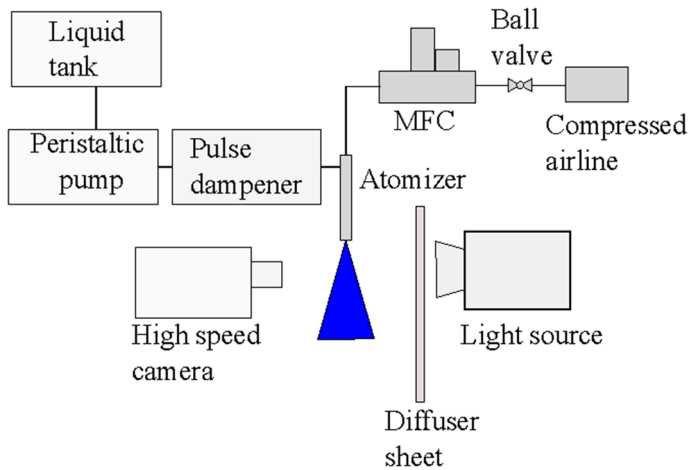**Fig. 2** Cross-sectional view of the atomizer

Fig. 3 Schematic diagram of the high-speed imaging setup

2.2 Optical Diagnostic Tools

Spray dynamics under various operating conditions are first investigated using a high-speed imaging setup. A schematic diagram of the experimental arrangement is shown in Fig. 3. It consists of a high-speed camera (Phantom VEO 710L, Vision Research) equipped with a Nikkor 50 mm lens (f/2.8) and a high-intensity LED (model 900445, Visual Instrumentation Corp.) unit. The LED light source provided a backlit illumination of 12,000 lm. A tracing paper is used to diffuse the light uniformly. The high-speed camera acquired 12-bit images at a pixel resolution of 800×448 pixels and a frame rate of 15,000 fps in the near field of the spray. The spatial resolution is about 20 microns per pixel. The exposure time is kept as 1 µs.

Phase Doppler particle analyzer is utilized to measure the diameter and velocity of the droplets simultaneously. A schematic diagram of PDPA setup is shown in Fig. 4. The PDPA system (TSI FSA 3500) consists of a transmitter unit, receiver optics and a signal processing unit. The transmitter unit generated a continuous laser beam of 500 mW at wavelengths of 532 nm and 561 nm. The 561 nm (light yellow) wavelength laser is used for axial velocity measurement, and the 532 nm laser (green color) is used for radial velocity measurement. The beam spacing between unshifted and shifted beams is 50 mm at each wavelength. The focal lengths of the transmitter and receiver optics are maintained at 362.6 mm and 300 mm, respectively. The scattering angle between the transmitter and receiver was set at 120 degrees. The receiver unit captured the scattered light from the droplet passing through the probe volume and focused on the photomultiplier tube. The output of the photomultiplier is converted to a voltage signal and processed by the FSA4000 multi-bit digital signal processor unit. The maximum droplet size that can be measured with the PDPA setup arrangement used in this work is 261 µm. The velocity ranges of the first and second channels are -5 m/s to 201 m/s and -38.2 m/s to 98.23 m/s, respectively. The uncertainty of the velocity measurement is 0.5%. The uncertainty of droplet diameter measurement is 1%. For each test condition, at least 10,000 valid droplets are captured to obtain reliable statistics.
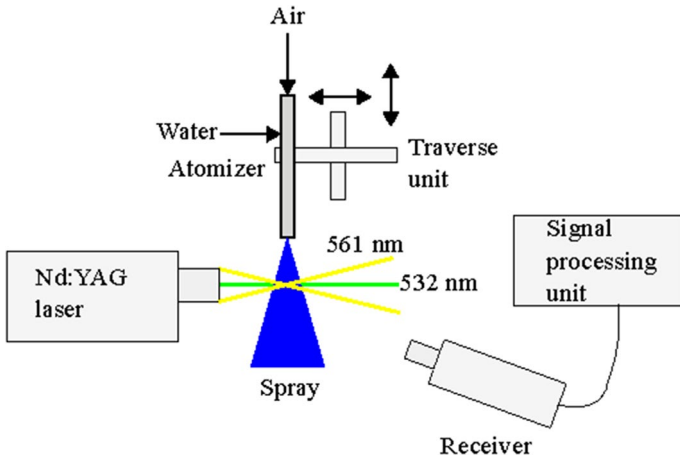
Fig. 4 Schematic diagram of the phase Doppler particle analyzer

Dimensionless numbers such as droplet Weber number (Eq. 1) and Reynolds number (Eq. 2) for droplets are calculated based on the axial velocity (U_d) and droplet diameter (D_d). Note that ρ_d is the density of water, σ is the surface tension, and μ_d is the dynamic viscosity of the droplets.

$$We_d = \frac{\rho_d \cdot U_d^2 \cdot D_d}{\sigma} \tag{1}$$

$$Re_d = \frac{\rho_d \cdot U_d \cdot D_d}{\mu_d} \tag{2}$$

2.3 Operating Parameters

The objective of this work is to establish a relationship between the spray formation mode and the operating parameters of the twin fluid atomizer. The test matrix has been optimized to achieve two different spray modes under various ALR and LFR conditions. These conditions are listed in Table 1. ALR is defined as:

$$\text{ALR} = \frac{\dot{m}_a}{\dot{m}_l} \tag{3}$$

where $\dot{m}_a$ is the mass flow rate of air and $\dot{m}_l$ is the mass flow rate of water. The Reynolds number of the liquid stream is defined as:

$$Re_l = \frac{\rho_l \cdot U_l \cdot D_l}{\mu_l} \tag{4}$$

where U_l is the characteristic velocity of the liquid, D_l is liquid tube diameter, ρ_l is the liquid density and μ_l is the liquid dynamic viscosity.

Table 1 Test matrix

Case No	LFR (mlpm)	Re_l	AFR (SLPM)	ALR
1	8	113	8.1	1.25
2			10.1	1.5
3			13.5	2
4	12	169	10.1	1
5			12.7	1.25
6			15.2	1.5
7	16	226	10.1	0.75
8			13.5	1
9			16.9	1.25

Three different LFR values (8 mlpm, 12 mlpm, and 16 mlpm) are considered, and the corresponding liquid Reynolds numbers are 113, 169 and 226, respectively. ALR values vary between 0.75 to 2 by regulating the AFR for various LFR. PDPA measurements are performed along the centreline of the spray (axial, $z = 10$ mm to 70 mm, 2 mm increments, $r = 0$ mm) and radial direction ($z = 50$ mm, $r = 0$ to 15 mm, 1 mm increments).

It may be noted that the operating parameters are investigating the lower limit of the pneumatic atomizer (refer Fig. 1) from the perspective of spray quality. Increasing AFR beyond the test matrix is expected to produce the fine spray as the input energy to the twin-fluid atomizer increases resulting in production of larger surface area which is realized to smaller droplets as surface area to volume increases with reduction in droplet diameter.

3 Results and Discussions

In the present study the operating parameter, atomizing air flow rate, is varied such that Mach number changes from 0.2 to 0.48 based on bulk mean velocity estimation to understand the lower limit for liquid and air flow rates from spray quality perspective.

3.1 Spray Modes

In a twin fluid atomizer, the injector geometry and operating parameters affect the presence of a liquid jet at the atomizer outlet. In this study, the geometric parameters were kept constant ($H/D = 0.2$) and the operating parameters varied. Two different spray forming modes based on liquid jet breakup, flow focusing (FF) and flow blurring (FB) were considered. In FF mode of spray formation, the liquid jet breaks at the exit of the atomizer, while in FB mode, the liquid jet breaks in the atomizer (Gañán-Calvo 2005).

High-speed imaging is performed to identify the mode of spray formation. Figure 5 shows high-speed images of near-field sprays under various operating conditions. The corresponding case number is listed on each image. Spray formation in FF mode is observed in case numbers 1, 2, 4, and 7, and spray formation in FB mode is observed in the remaining cases. In FF mode cases, the liquid jet is visible near the exit of the atomizer and primary breakup is observed after $z = 2$ mm. However, in the case of FB, the liquid ligament is visible at the exit itself, and further secondary breakup is seen downstream. In some FF cases, we can observe bag breakup mode, as in the images of cases 2 and 4. The presence of bigger droplets is more visible in the case of FF compared to the case of FB and

Fig. 5 High-speed images of liquid sprays under various operating conditions. FF mode is observed in case numbers 1, 2, 4 and 7. FB mode is observed in case numbers 3, 5, 6, 8 and 9
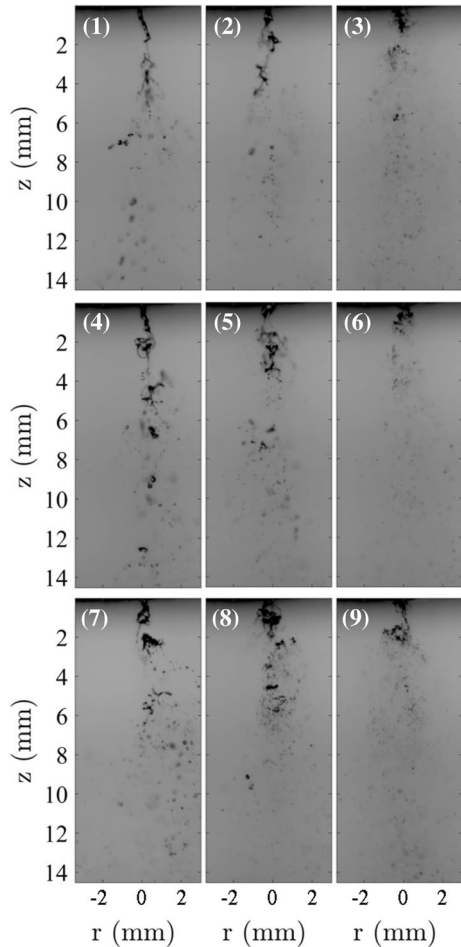
indicates that the FB mode produced more fine droplets. Note that for all cases downstream of $Z = 10$ mm only droplets are present and PDPA measurements were carried out from $Z = 10$ mm and downstream.

Figure 6 shows the superposed images from the set of 8833 instantaneous images at different operating conditions similar to Fig. 5. From Fig. 6, it is evident that for cases 1, 2, 4, and 7 spray spread changes suddenly in near field region without the exit orifice running full indicating liquid jet focusing and flapping jet instability and is identified as the flow focusing mode of operation. For other cases, spray spread at dump plane is nearly the same as exit orifice diameter and cone angle is not observed to change suddenly indicating jet breakup occurred internally and hence flow blurring mode of operation is confirmed in cases 3, 5, 6, 8, 9. For operating conditions for case 6, AFR is the highest and the superposed image indicates the mist type of spray quality. Note that for line of sight technique in high-speed imaging, finer droplets would permit more light intensity to pass through and can be used to qualitatively judge the spray quality.

All cases are classified into FF mode and FB mode based on qualitative observation from high-speed images and superposed image construction and is shown in Fig. 7. The
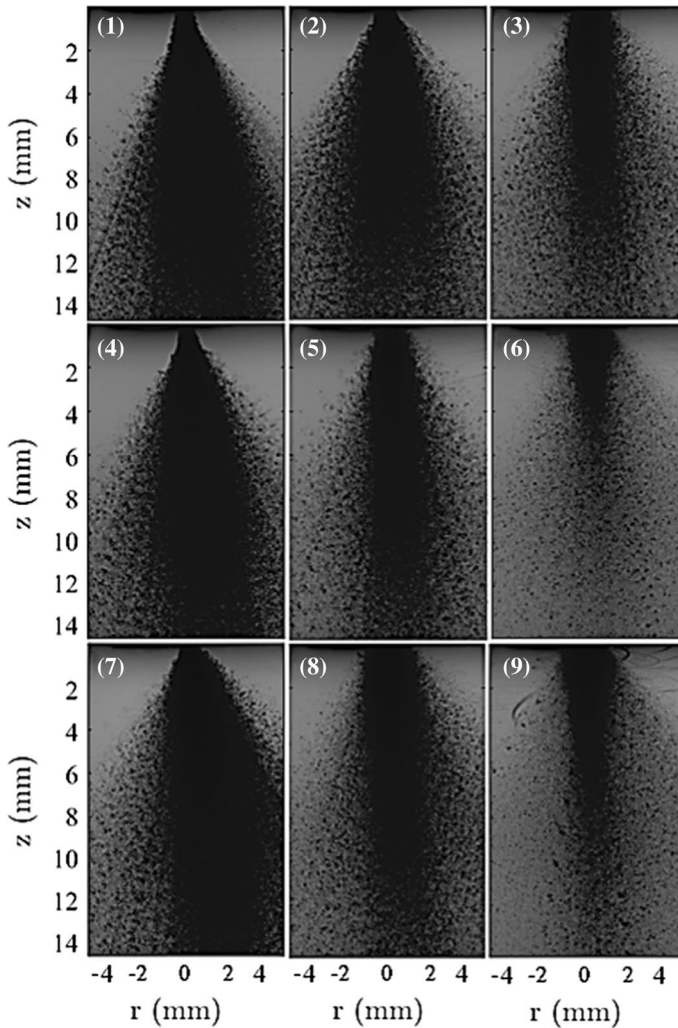
Fig. 6 Spray spread with superposed images from high speed imaging. FF mode is observed in case numbers 1, 2, 4 and 7. FB mode is observed in case numbers 3, 5, 6, 8 and 9

dashed line indicates the branch between FF mode and FB mode. If LFR is low, a transition from FF mode to FB mode occurs when ALR is high. As the LFR increases, the energy transfer from the air stream to the fluid stream increases, bifurcates at a lower ALR.

3.2 Effect of AFR on Spray Characteristics

3.2.1 Spray Characteristics at Centreline

Twin fluid atomizers operate on the principle of exchanging energy from one fluid to another and atomizing the liquid into droplets. Operating parameters play an important role

Fig. 7 Two spray modes with different ALR and three different LFR
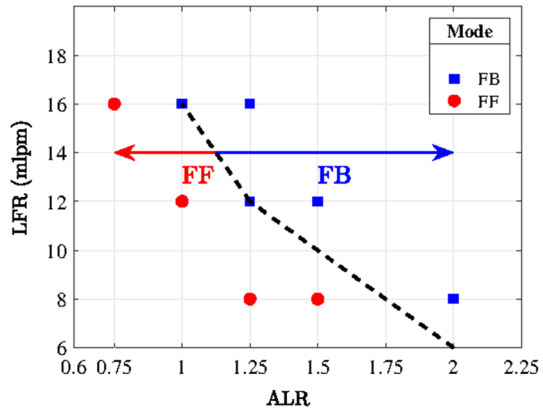
in determining the efficiency of the atomizer, as spray formation in FF or FB mode can occur. In this work, we will first investigate the effect of AFR on spray characteristics by maintaining LFR = 12 mlpm and changing AFR from 10.1 slpm to 15.2 slpm. The corresponding ALR varies from 1 to 1.5. FF mode is observed with ALR = 1. As AFR increased from 10.1 slpm to 12.7 slpm, mode transitions were observed, and as AFR increased further to 15.2 slpm, the FB spray formation mode was well established.

Figure 8 shows mean droplet sizes and velocities for three different AFR conditions at fixed LFR along the spray centreline. At z = 10 mm, Case 4, in FF mode produced larger droplets compared to Cases 5 and 6 operating in FB mode. In addition, in the FF mode, the presence of the ligament increased the droplet size to 30 mm downstream and the ligament began to break further, reducing the SMD from about 92 microns at 30 mm to about 80 microns at 70 mm. The MMD of the droplet showed a similar trend as the SMD. In the case of FB, the droplet size is about 75 microns at 10 mm, and the size decreases downstream due to the secondary fragmentation of the droplets. As the AFR increases, the size reduction becomes more pronounced as the momentum exchange between the airflow and the water improves. Again, in Cases 5 and 6, the MMD of the droplets showed a similar trend as observed with SMD. For a given LFR, increasing the AFR from 10.1 slpm to 15.2 slpm results in droplet sizes of about 90 to about 60 microns each.

The mean axial velocity of the droplet along the centreline is shown in lower left corner of Fig. 8. The corresponding RMS velocity profiles calculated from the PDPA measurement are shown in the lower right corner of Fig. 8. The mean droplet velocity in FF mode is the lowest compared to FB mode. Case 4 also has the lowest RMS velocity. This is because larger droplets have higher inertia and higher slip velocity. The fine droplets generated in cases 5 and 6 operating in FB mode have higher velocities and can follow turbulence faithfully, as indicated by higher RMS velocities downstream. Comparing Cases 5 and 6, it can be seen that as the AFR further increased, the axial velocity at the atomizer outlet increased and began to merge again downstream. As shown, the higher the AFR and the higher the level of the RMS velocity, the finer the droplet that can follow the turbulence. Higher mean and RMS values for FB mode are attributed to higher AFR and energy transfer from air to liquid. Interestingly, mean diameter shows the distinction between FF and FB mode trend along the spray centreline variation. For flow focusing mode, droplet size decrease is not observed in near field region which can be attributed to droplet coalescence and ligament presence in flapping instability exhibited in FF mode. Additionally, at
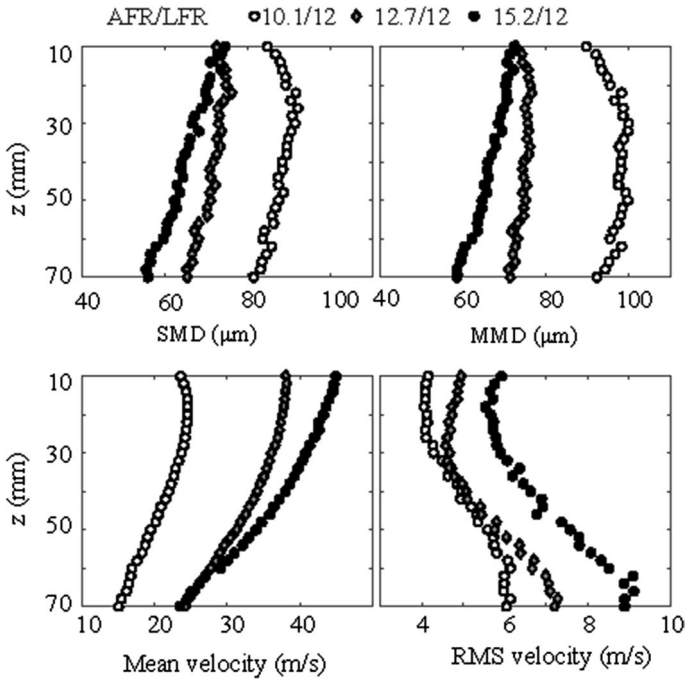
Fig. 8 Variation in SMD, MMD, mean velocity and RMS velocity of droplets along the centreline of various AFR sprays with constant LFR

$Z = 10$ mm, mean droplet diameter (MMD) exceeds 90 µm was observed for flow focussing mode of operation. With increase in AFR, FF to FB mode transition occurs and sharp decrease in droplet diameter can be attributed to very high aerodynamic strain exerted by high-speed atomizing air.

Figure 9 shows the probability density function(PDF) of the droplet at $z = 10$, 30, and 70 mm for three different AFRs with a constant LFR. At $z = 10$ mm, the peak value for the FB case is about 51 microns and the FF case is about 55 microns. The distribution of the FF case is wider than that of the FB case, indicating that large droplets are present in the FF mode. Along the downstream, the peak values in all cases shift to smaller diameters, narrowing the distribution at $z = 70$ mm. The difference between Case 4 and Case 5 is minimal at $z = 70$ mm. The cumulative distribution function (CDF) at $z = 10$ mm shows an overlap of FB cases 5 and 6. For FB, 50% of droplets by counting is about 55 microns, and 90% of droplets by counting is about 77-80 microns. However, for FF, 50% of the counted droplet is about 62 microns and 90% of the counted droplet is about 98 microns. The smallest droplet size is observed in Case 6. The RSF values in all cases are approximately 0.92–1.12, indicating uniformity of the droplet size distribution. With an increase in AFR, PDF amplitude increases and shifts towards smaller droplet diameters along with a reduction in shape factor indicating finer spray. This can be attributed to a higher supply of kinetic energy of atomizing air getting dissipated as droplet surface energy in creating a multiplicity of droplets from liquid jet or ligaments.

Probability distributions in the near field ($Z = 10$ mm) for FB cases (AFR = 12.7 slpm and 15.2 slpm) seems much alike, however a discrepancy is observed at downstream
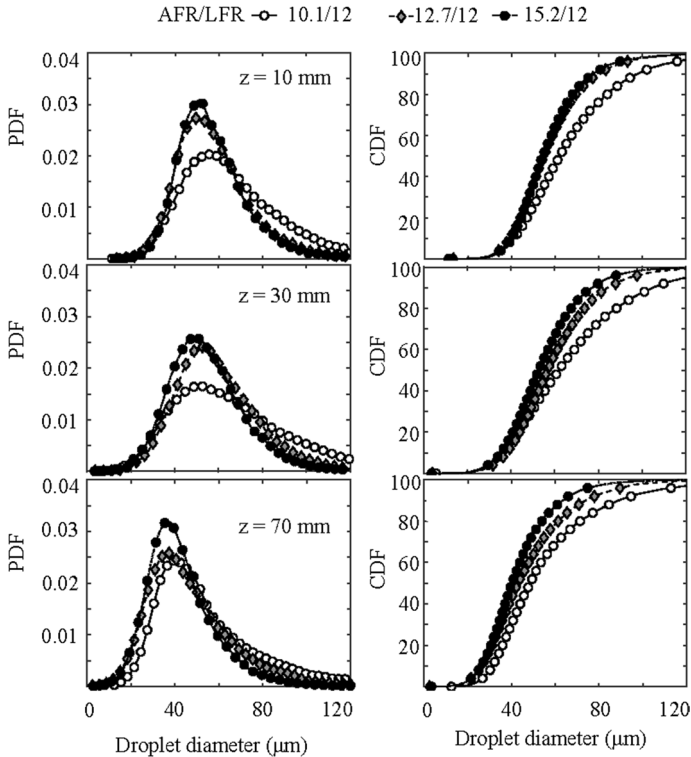
Fig. 9 PDF and CDF of droplets at z = 10, 30, and 70 mm for various AFRs with constant LFR. Note that bin size employed for droplet diameter is 1 μm to estimate its PDF

locations say Z = 70 mm. This can be attributed to the portion of energy dissipated in entrainment is different due to the difference in velocity gradient. For higher ALR, the velocity gradient with ambient air is expected to be higher and droplets would be influenced by the entrainment and follow curvilinear motion (refer Fig. 6 test cases 6 and 9). Curvilinear motion leads to a lowering of requirement Weber number for secondary breakup of droplet diameter (Soni et al. 2020). This would explain in the change in the PDF distribution, amplitude and shape observed in Fig. 9. It is evident that the shape for FF mode follows more heavy-tailed distribution (or larger droplets). It can be concluded that change in AFR alters the probability distribution irrespective of FF or FB mode of operation of the atomizer. Note that in FF mode the PDF shape shows heavy tailed distribution indicating difference in underlying distribution.

Figure 10 shows the combined probability distribution function of droplet diameter and velocity at two different axial positions (z = 30 mm and 70 mm) along the centrelines of Cases 4, 5, and 6. JPDF captures the effect of flow field on droplet size and velocity in the spray developing region. FF mode shows longer tail end at lower velocity range compared to FB mode. Due to the high secondary breakup and the high mass flow of air, the droplets move faster in FB mode than in FF. Between FB cases, the increase in axial velocity in the small drop size range of Case 6 is due to a further increase in AFR. At z = 70 mm, bimodal distributions are observed in all three cases is attributed to entrainment flow feature and
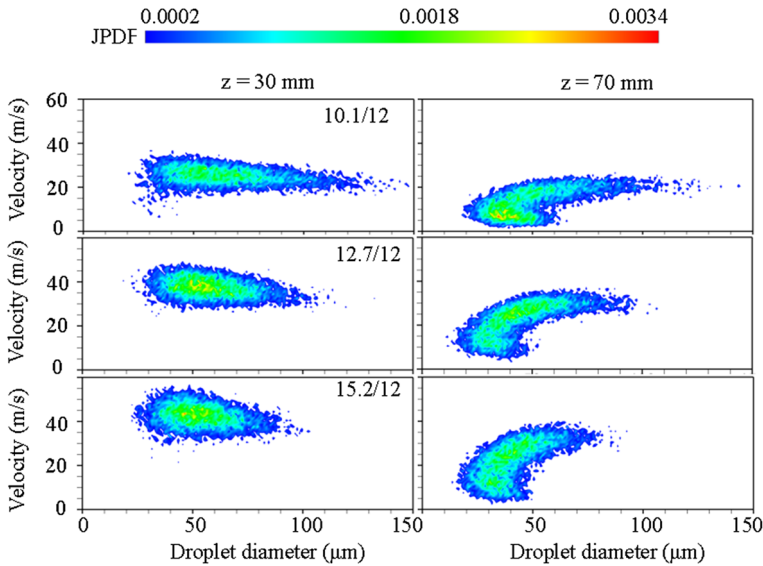
Fig. 10 JPDF of droplet diameter and axial velocity at two different axial positions of different AFR with constant LFR. Note that bin sizes employed for droplet diameter and velocity are 1 μm and 1 m/s respectively to estimate the JPDF

radial spread of the spray resulting in droplets of the same size traveling at two different velocities during the PDPA probe-volume sampling duration. Again, Case 6 shows a higher velocity and a narrower droplet size distribution than Cases 5 and 4 due to better atomization and increased bulk velocity.

The combined distribution of droplet Weber number and Reynolds number is shown in Fig. 11 for two different axial positions ($z = 30$ mm and $z = 70$ mm). At $z = 30$ mm, the slope in FB mode is steeper than in FF mode. This is due to the faster and finer droplets that are generated when the secondary breakup increases. Case 6 has the highest gradient, indicating good atomization. A similar trend is observed at $z = 70$ mm in all three cases. The peaks in the distribution shift to lower We and Re for both FF and FB mode due to finer droplets traveling at lower velocities going through the secondary breakup process.

3.2.2 Spray Characteristics Along the Radial Direction

Radial spray properties play a key role in understanding the penetration, and entrainment of droplets by the surrounding air. Figure 12 shows various spray parameters measured radially 50 mm downstream of the atomizer outlet. In FF mode, droplet coalescence and poor secondary atomization increase droplet SMD and MMD from the centreline toward the spray edge. However, in the case of FB, SMD, and MMD decrease continuously along the radial direction due to improved secondary breakup. Case 6 generated smaller droplets, aided by higher momentum from the airflow. The mean velocity trend is similar to that described for centreline spray characteristics. Again, the FF case has the lowest velocity of all droplets due to the larger size range compared to the FB case. There is no difference in mean velocity between cases 5 and 6, but the RMS value increases with higher AFR.

Figure 13 shows the spray droplet PDF and CDF at three different radial positions with different AFR at a constant liquid flow rate. At the centreline (top row), the spray behavior
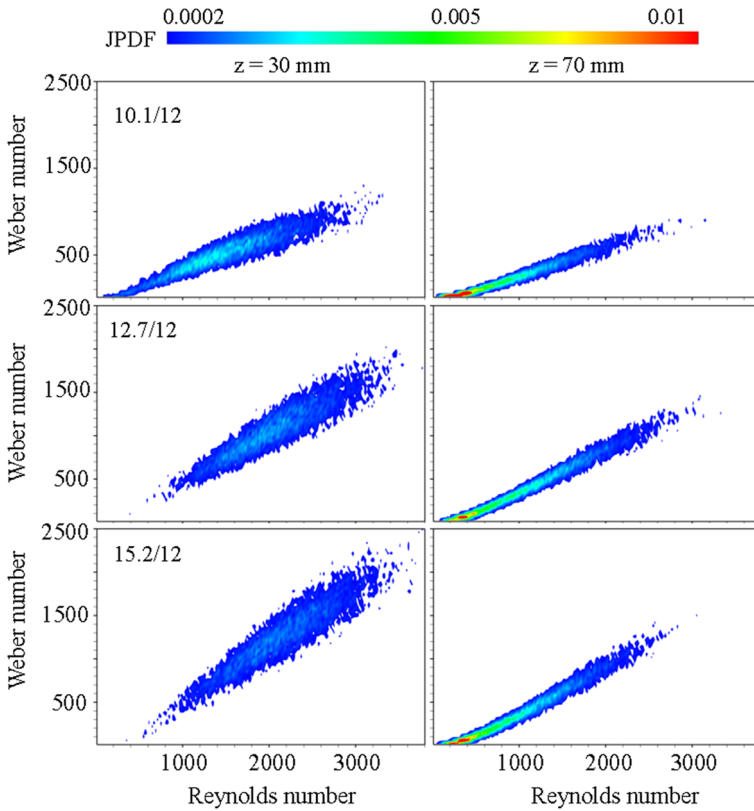
Fig. 11 JPDF of Reynolds number and Weber number at two different axial positions of different AFR with constant LFR. Note that bin sizes employed for Reynolds and Weber numbers are 20 and 40 respectively to estimate the JPDF

is similar to Fig. 9. For outer radial location, the peak probabilities increase and probability distribution shifts toward smaller droplet sizes by narrowing the distribution in all three cases. The FB case produces finer droplets compared to the FF case with the longer tail end of larger droplets at $r = 12$ mm. Case 6 droplet CDF peaks faster because it produced finer droplets than the other two cases. In FF mode, large droplets were generated everywhere, as seen in the corresponding PDF curves. Therefore, FF mode has the smallest area under the CDF curve, and Case 5 lies between Cases 4 and 6. D_{90} defined as the diameter corresponding to CDF of 90% is significantly larger ($D_{90} \approx 100$ μm) for FF mode and can be used as distinguishing parameter to identify FF mode from FB mode of operation ($D_{90} < 80$ μm).

Figure 14 shows the combined probability distribution function of droplet diameter and velocity at two different radial positions ($r = 0$ mm and 6 mm) 50 mm downstream of Cases 4, 5, and 6. It is evident that JPDF captured the secondary breakup process through shift in distribution from larger droplets to smaller droplets. Besides, entrainment and spread influence is captured through the reduction in droplet velocities. At the centreline ($r = 0$ mm), JPDF starts to display the bimodal distribution of all cases better established at $z = 70$ mm (Fig. 10). In each case, moving radially outward, the droplet velocity decreases faster than
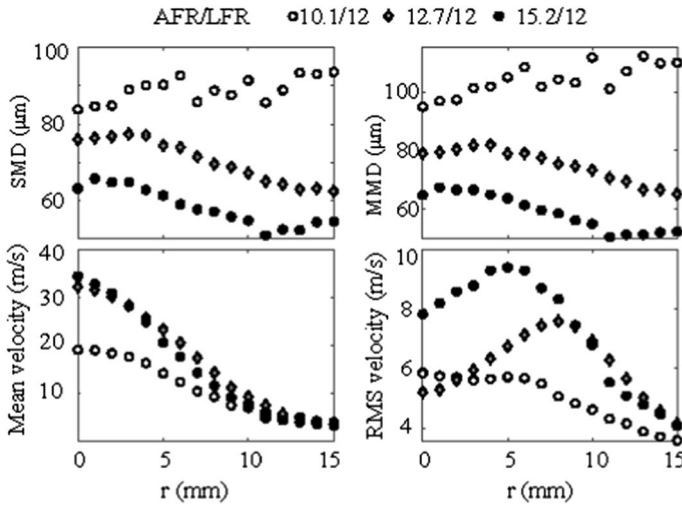
Fig. 12 Variation of SMD, MMD, mean velocity, and RMS velocity of droplets 50 mm downstream of various AFR sprays with constant LFR
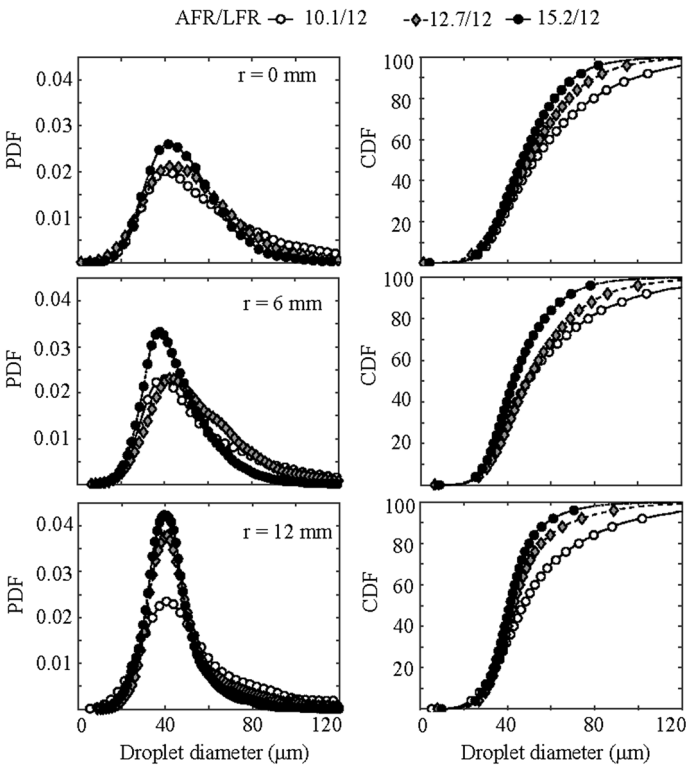

Fig. 13 PDF and CDF at three different radial locations 50 mm downstream of different AFRs with constant LFR. Note that bin size employed for droplet diameter is 1 μm to estimate its PDF
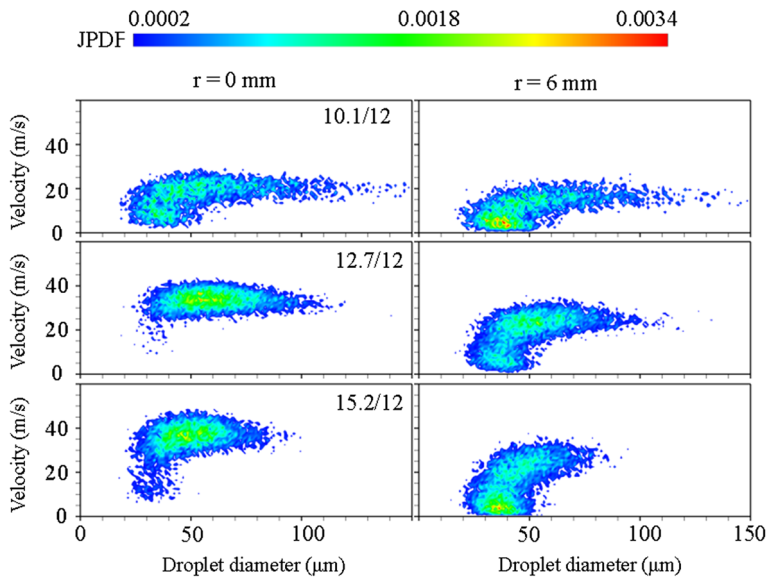
Fig. 14 JPDF of droplet diameter and velocity at two different radial positions of different AFR with constant LFR. Note that bin sizes employed for droplet diameter and velocity are 1 μm and 1 m/s respectively to estimate the JPDF

the corresponding size reduction, favoring bimodal distribution at outer radial locations compared to the centreline. The tail of the distribution shrinks with increasing AFR due to better atomization.

The combined distribution of droplet Weber number and Reynolds number is shown in Fig. 15 for two different radial positions (r=0 mm and 6 mm) 50 mm downstream of Cases 4, 5, and 6. In FF mode, the JPDF peak is near the low Weber number and Reynolds number at both locations. The distribution is similar in both places because the variation in velocity range is similar to the SMD range at r=0 and 6 mm (Fig. 12). However, in FB mode, improved atomization increases the gradient of the distribution with increasing AFR, producing faster, finer droplets. Moving radially outward reduces both size and velocity, and reduces the slope of the distribution.

3.3 Effect of LFR on Spray Characteristics

3.3.1 Spray Characteristics at the Centreline

In most literature, the operation of twin-fluid atomizers is mainly studied based on ALR (Lefebvre 1980, 1989; Nukiyama and Tanasawa 1938; Murugan et al. 2018; Gañán-Calvo 2005; Simmons et al. 2009; de Azevedo et al. 2016; Khan et al. 2019; Groom et al. 2005; Panchasara et al. 2009; Panchasara and Agrawal 2010; Simmons and Agrawal 2012; Agrawal et al. 2013; Kourmatzis et al. 2016; Kulkarni and Deshmukh 2017; Gad et al. 2018; Raju et al. 2018). Different AFR and LFR combinations can be used as operating parameters for the same ALR. As we saw in the previous section, AFR significantly
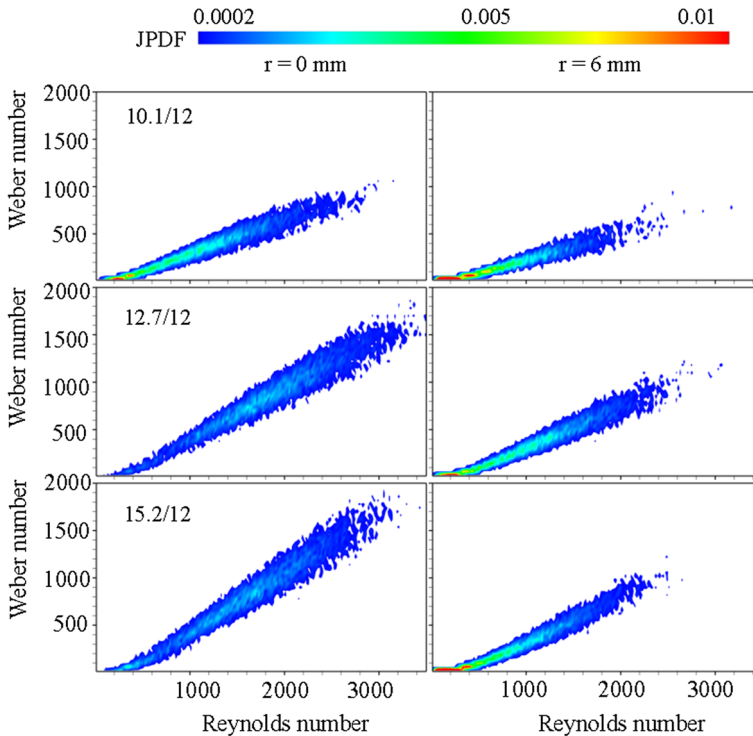
Fig. 15 JPDF of Reynolds number and Weber number at two different radial positions of different AFR with constant LFR. Note that bin sizes employed for Reynolds and Weber numbers are 20 and 40 respectively to estimate the JPDF

changes the spray characteristics of certain LFR. In this section, we examine the effect of LFR by keeping AFR constant.

Figure 16 shows the SMD, MMD, Mean, and RMS velocities of the droplets along the centreline of the spray in Cases 2, 3, 7, and 8. Cases 2 and 7 belong to FF mode and cases 3 and 8 belong to FB mode. With AFR = 10.1 slpm, as LFR increases from 8 mlpm to 16 mlpm, SMD and MMD show the same droplet size variation downstream. So, irrespective of LFR, for same AFR FF mode observed indicates the flow bifurcation (Murugan et al. 2018; Gañán-Calvo 2005) and hence the jet breakup did not occur internally and the AFR was lower than threshold AFR for given H/D ratio. Similarly, keeping the AFR constant at 13.5 slpm and doubling the LFR value resulted in the same drop size variation. Again, FB mode produces finer droplets than FF mode, indicating that secondary breakup is more pronounced in FB mode. Mean and RMS velocity plots show higher values in FB mode than in FF mode. Again, the bulk velocity of the spray droplets is affected by the AFR, so the effect of the LFR is minimal. It may be noted that the atomizing air is the source of energy supplied, which is dissipated in creating surface energy as well as entrainment. Hence, for same AFR the mean droplet size variation shows the very similar trend throughout the spray developing region.

Figure 17 shows the PDF and CDF of the droplet measured at three different axial locations. At z = 10 mm, the peak value is higher in FB than in FF due to the narrow
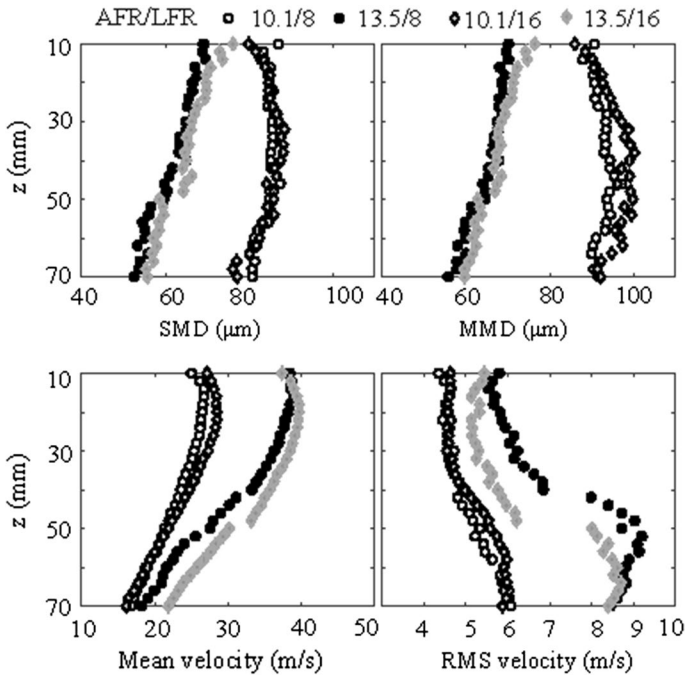
Fig. 16 Variations in SMD, MMD, mean velocity, and RMS velocity of droplets along the centreline of two different LFR and AFR combinations

distribution. However, a closer look at the PDF shows that Case 3 and Case 7 droplet sizes overlap up to about 35 microns, and Case 7 diverges due to the long tail. The same trend observed at $z = 70$ mm, where cases 3, 7 and 8 overlaps up to about 30 microns and then case 7 diverged. The same trend is seen at $z = 70$ mm, with PDFs in Cases 3, 7, and 8 overlaps by about 30 microns, after which Case 7 diverges.

CDF profiles at various locations show a similar overlap of cases up to certain droplet size and diverge in FF mode. At $z = 70$ mm, for FB, 50% of droplets by counting is about 36-38 microns, and 90% of droplets by counting is about 57-62 microns. However, cases 2 and 7 (FF mode) produce different ranges of droplet sizes. In case 2, 50% of the counted droplet is about 49 microns and 90% of the counted droplet is about 90 microns. In case 7, 50% of the counted droplet is about 38 microns and 90% of the counted droplet is about 80 microns. The difference in size range produced by two different LFRs with a constant AFR indicates that in FF mode, increasing LFR produces finer droplets. In all cases, the relative span factor of the spray droplets ranged from 0.83 to 1.19.

Figure 18 shows the combined probability distribution function of droplet diameter and velocity at two different axial positions along the centrelines of Cases 2, 3, 7, and 8. In general observations, large droplets with a smaller velocity range were generated in FF mode than in FB mode. For the same LFR value, two different spray patterns were generated for two different AFRs. Doubling the LFR of the same AFR doubles the ALR, but the spray mode remains the same regardless of the ALR change, so the spray characteristics remain the same. The combined probability distribution function of Weber
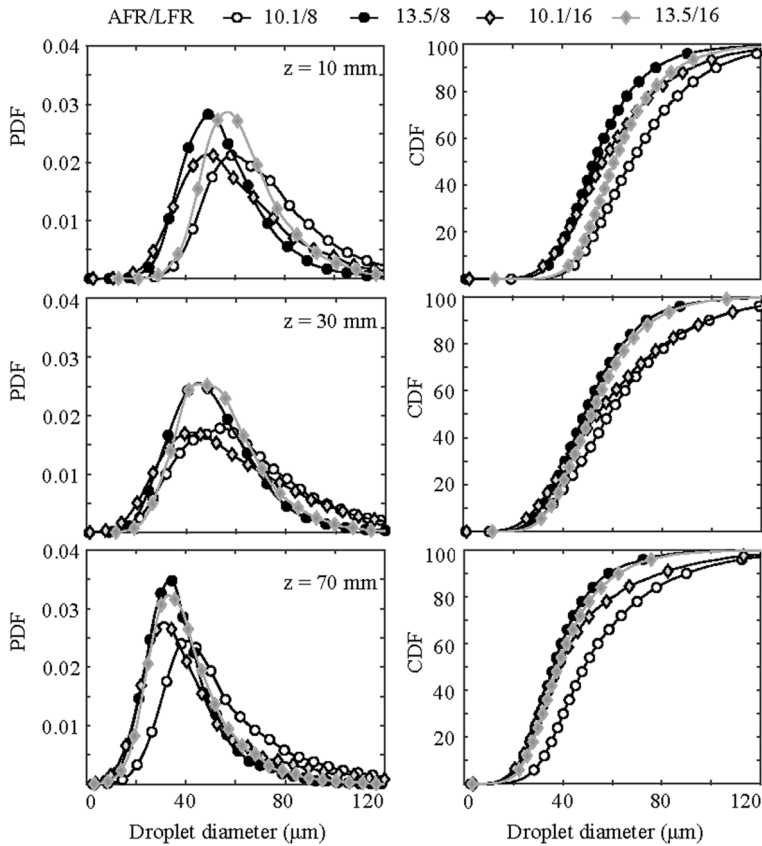
Fig. 17 PDF and CDF of droplet diameter at three different axial positions. Note that bin size employed for droplet diameter is 1 μm to estimate its PDF

number and Reynolds number of the droplet at two different axial positions along the centreline of cases 2, 3, 7, and 8 are shown in Fig. 19. Again, similarities are observed between cases operating in the same mode. This confirms that spray modes are more dominant in determining spray characteristics than LFR values. Therefore, selecting the correct AFR and maintaining the spray mode at the FB will provide uniform spray characteristics at various LFR values.

3.3.2 Spray Characteristics Along the Radial Direction

Figure 20 shows various spray parameters measured radially 50 mm downstream of the atomizer outlet for two different AFR/LFR combinations. Along the radial direction, FF mode produces droplets in the size range of about 90 ± 10 microns, while FB mode produces droplets of approximately 60 ± 8 microns. FF mode has a similar mean velocity plot for two different LFRs, but in FB mode, the mean velocity increases moderately with the LFR. The RMS velocity plot shows a similar trend as observed for the mean velocity. In the case of FF, the velocity fluctuation is smaller than the FB velocity fluctuation.
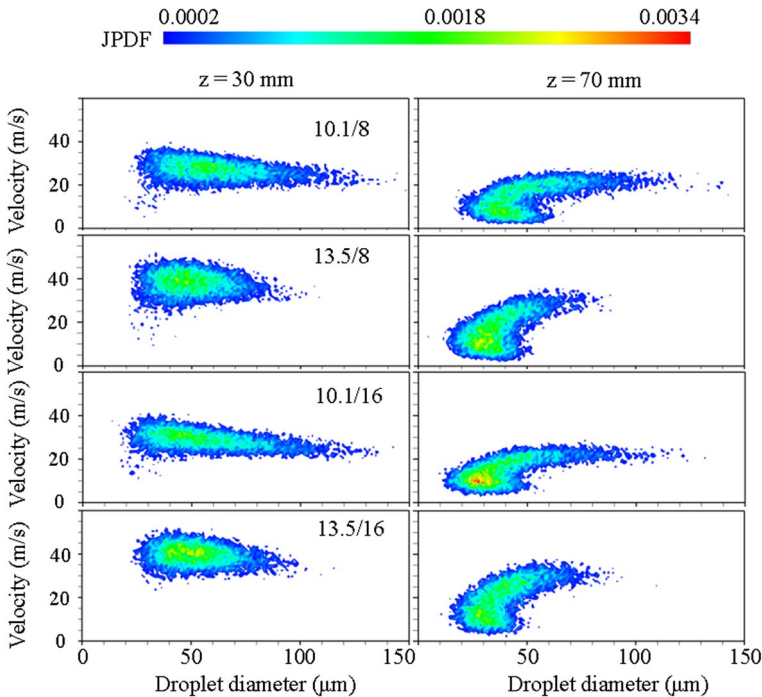
Fig. 18 JPDF of droplet size and velocity at two axial positions. Note that bin sizes employed for droplet diameter and velocity are 1 μm and 1 m/s respectively to estimate the JPDF

Figure 21 shows the spray droplet PDF and CDF at three different radial positions for two different AFR/LFR combinations. At the centreline, FB mode has the same droplet size distribution at two different LFRs. However, in FF mode, increasing LFR produces smaller droplets and shifts the distribution peak to smaller droplet sizes. The corresponding CDF profile confirms the trend. At r = 6 mm, the peaks in the distribution for all cases shift to smaller droplet sizes, and the CDFs for cases 2 and 7 overlap each other. Similarly, the CDF profiles of cases 3 and 8 overlap each other. The same pattern is observed at r = 12 mm. This indicates that the mode of operation is more important than the variation of ALR.

3.4 Fitting of Probability Distribution Function to Experimental Data

Droplet diameter probability distribution shows significant shift in distribution to lower diameters as FF mode is switched to FB mode operation of the atomizer. Besides, other than spray centreline in the near field for different AFR conditions but same mode of operation, the droplet size distribution shows very similar peak probabilities and spread but this discrepancy increases at far downstream or radially outward location as the velocity gradient influence affects the ambient entrainment; consequently, different distribution is observed in such cases (refer Figs. 9, 13, 17 and 21). Kooij et al. (2018) have proposed the two parameter compound gamma distribution to account for variation in observed droplet PDF for flat fan and conical nozzles that deal with sheet breakup. The scope of this section
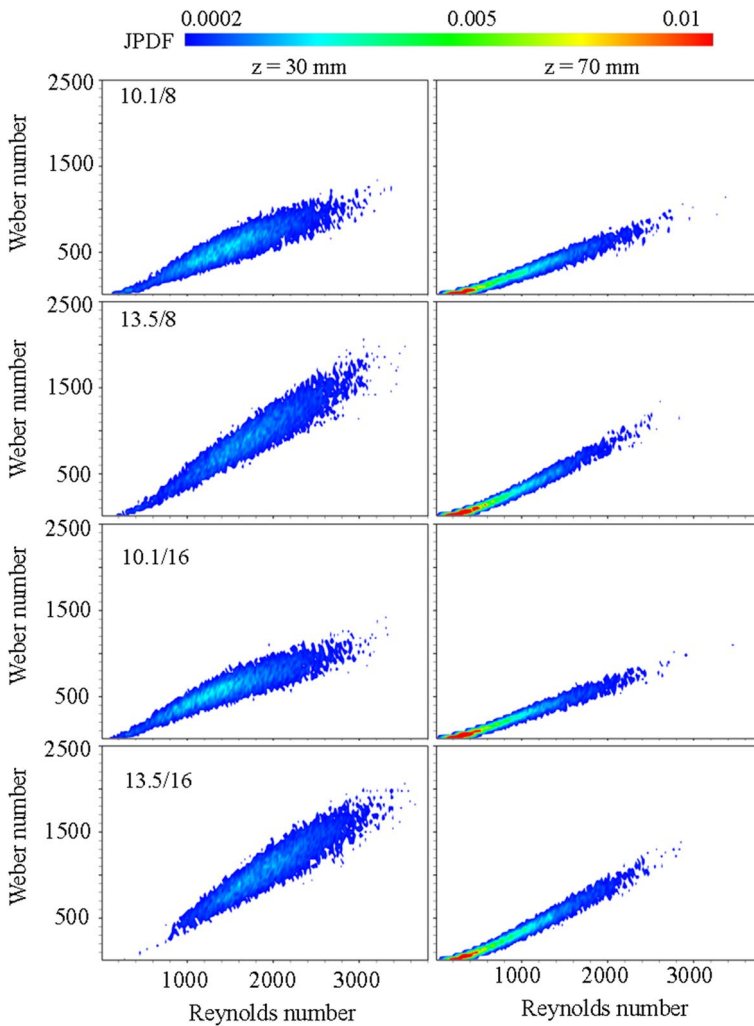
Fig. 19 JPDF of Reynold number and Weber number at two axial positions. Note that bin sizes employed for Reynolds and Weber numbers are 20 and 40 respectively to estimate the JPDF

is to find a way to represent the experimentally observed droplet diameter distribution with high confidence level. Exercise of fitting lognormal, beta or gamma distribution experimental data made it clear that the confidence level for approximating the experimental PDF varies with droplet bin size itself although lognormal distribution closely mimics the experimentally observed distribution.

Secondary atomization process in a spray developing region can be seen from the perspective of parent droplets distribution and child droplet distribution. The observed droplet distribution using the PDPA technique would involve the combined distribution of such parent and child droplets and hence attempt was made to use two overlapping Gaussians to curve fit the observed droplet size probability distribution. Figure 22 shows a histogram and double overlapping Gaussian function aptly fitting the experimental data with a very high confidence level. Equation (5) represents the probability distribution function employed for
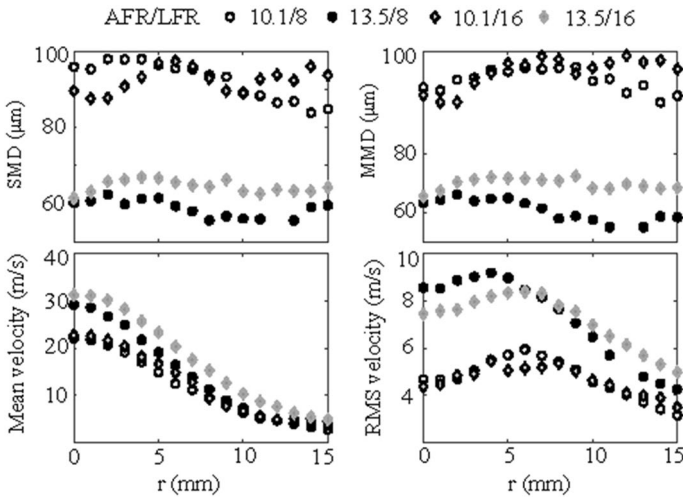
Fig. 20 Variation of SMD, MMD, mean and RMS velocity of droplets 50 mm downstream of two different AFR/LFR combinations
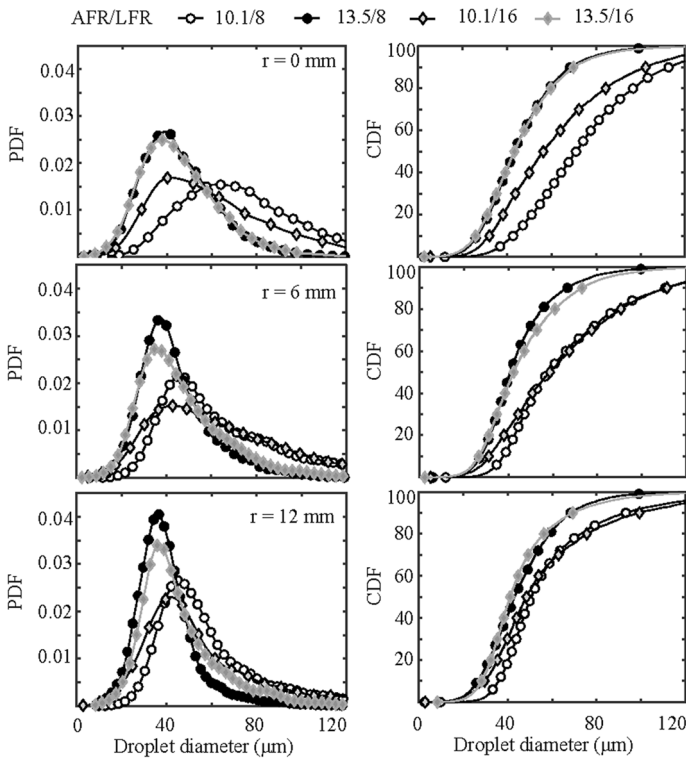

Fig. 21 PDF and CDF of droplet diameter at three different radial locations. Note that bin size employed for droplet diameter is 1 μm to estimate its PDF
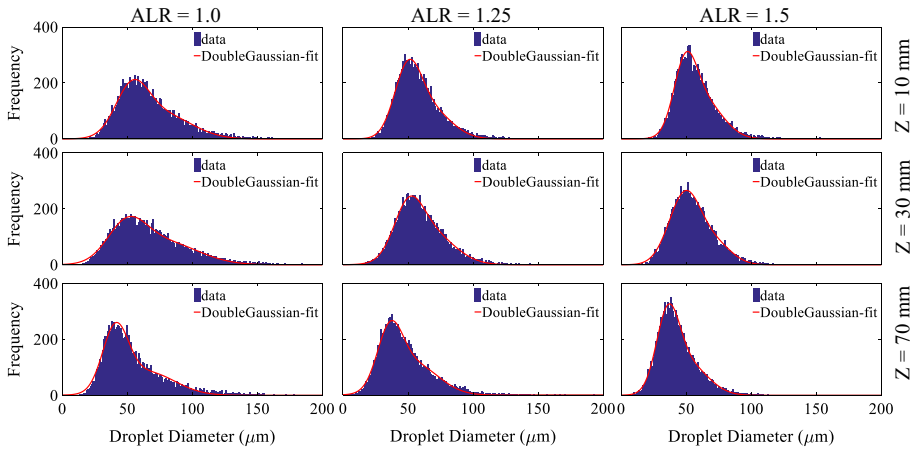
Fig. 22 Double Gaussian PDF fitting to the experimental data. Axial locations for each row are specified by Z values on right side and the ALR conditions for each column are specified by ALR values on top. Note that bin size employed for droplet diameter is 1 μm to estimate its histogram

fitting the observed droplet size distribution where parameters a_1, a_2 are amplitude factors and c_1, c_2 are shape factors for Gaussian with means centered at droplet diameter $\langle D_d \rangle_1$ and $\langle D_d \rangle_2$. Note that D_d represents droplet diameter.

$$P(D_d) = a_1 \times e^{-\{(D_d - \langle D_d \rangle_1)/c_1\}^2} + a_2 \times e^{-\{(D_d - \langle D_d \rangle_2)/c_2\}^2} \tag{5}$$

Figure 23 shows how various distribution fits the experimentally observed droplet diameter probability distribution. Best fit to worst fit order follows as double overlapping Gaussian, lognormal, gamma and then beta distribution. Further it was observed that other than
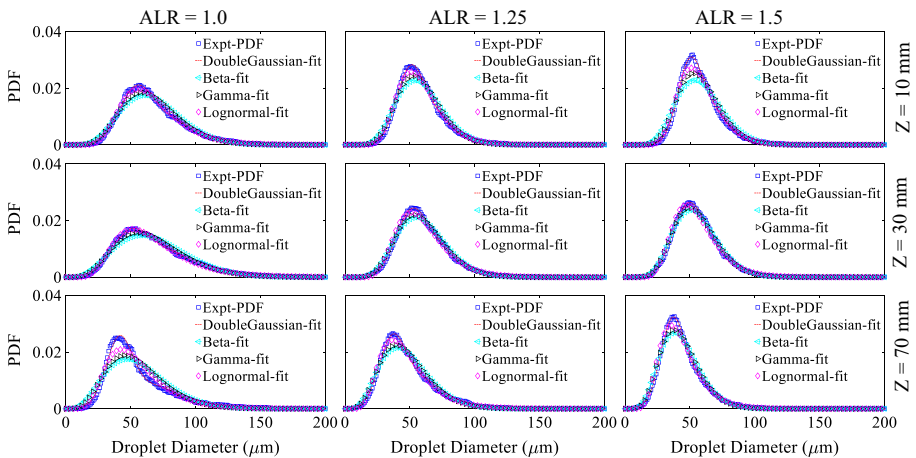

Fig. 23 Different probability distributions fitting to experimentally observed droplet distribution. Axial locations for each row are specified by Z values on right side and the ALR conditions for each column are specified by ALR values on top. Note that bin size employed for droplet diameter is 1 μm to estimate its PDF

Table 2 Mean droplet sizes for smaller and larger droplets in fitted overlapped Gaussian distributions

Operating ALR	Z = 10 mm		Z = 30 mm		Z = 70 mm	
	$\langle D_d \rangle_1$ (µm)	$\langle D_d \rangle_2$ (µm)	$\langle D_d \rangle_1$ (µm)	$\langle D_d \rangle_2$ (µm)	$\langle D_d \rangle_1$ (µm)	$\langle D_d \rangle_2$ (µm)
1	53.59	77.77	49.64	78.68	40.84	65.33
1.25	49.76	66.49	50.2	65.62	36.09	55.21
1.5	49.22	63.46	59.7	59.68	35.93	51.14

double overlapping Gaussians, all other distributions confidence level for fitting the experimentally observed probability distribution changes with bin size employed to find the droplet probability distribution. Table 2 shows the two means of Gaussian functions employed to fit the experimentally observed probability distribution for the test cases shown in Fig. 23. For FF mode operation observed at ALR = 1 test case clearly shows droplet distribution shifting towards larger droplets compared to smaller droplets and difference in the means of the two Gaussians reduces with increase in ALR. Variation in the means of the two Gaussians changes with AFR or axial distance indicating change in probability distribution. This observation similar to reported by Kooij et al. (2019).

4 Conclusions

In this study, we investigated the spray characteristics of a twin fluid atomizer using high-speed imaging and PDPA technique. Experiments are performed at room temperature of about 298 K, using air and water as the two working fluids. Spray mode is identified from high-speed images. PDPA is used to measure droplet size and velocity simultaneously. The geometric parameters of the atomizer are kept constant (H/D = 0.2), and the operating parameters are varied. Since the spray characteristics depend on the momentum exchange between fluids, the AFR and LFR are independently varied for the investigation. The following important conclusions can be drawn based on the experimental results:

- Spray spread at orifice exit and sudden change in spray spread with an axial location in near field characterize the FF mode of operation of the pneumatic injector considered. Another features of the FF mode operation are that MMD does not decrease in the immediate downstream region and the D_{90} observed is about 100 µm at axial location of Z = 50 mm.
- Below threshold AFR, absence of internal flow bifurcation results in flow focusing mode. Alternatively, for a given H/D ratio, AFR dictates the FF to FB mode transition instead of ALR.
- AFR as an operating parameter plays an important role in spray characteristics as observed from minimal effect of the LFR at a constant AFR on spray properties. For fixed atomizing air the operating mode (FF or FB) is same irrespective of LFR and the same mean droplet size variation also indicates the flow field structure effects (such as entrainment of ambient air) are similar as the velocity gradients change for the continuous phase would be insignificant.
- Doubling the LFR for the same AFR produces the same spray mode and the same droplet size and velocity distribution. Increasing the AFR from 10.1 slpm to 13.5 slpm shifted the spray mode of the two different LFRs (8 mplm and 16 mlpm) from FF to

FB. This indicates that the energy exchange between the atomizing air stream and the liquid stream is primarily governed by the air stream to produce the spray.

- In the case of FB mode of operation, the droplets SMD and MMD decrease linearly along the axial direction due to secondary breakup and entrainment based curvilinear motion at downstream, which reduces the threshold breakup Weber number.
- The JPDF characterizes the flow field effect on secondary atomization, which is evident from the shift in distribution to in droplet size and velocity as well as the transition from a unimodal to a bimodal distribution. This observation is observed in the both axial and radial direction downstream of the axial location of 50 mm.
- Overall, keeping the LFR constant at 12 mlpm and changing the AFR from 10.1 slpm to 15.2 slpm reduced the droplet SMD by 31% and increased the axial velocity by 40%. Higher momentum exchange from the air stream to the liquid stream improved secondary atomization, resulting in finer and faster droplets, as confirmed by the JPDF distribution of Weber number as a function of Reynolds number.
- Double overlapping Gaussians aptly describe the experimentally observed droplet size probability distribution, which is unaffected by a change in bin size employed for PDF estimation unlike lognormal, gamma, and beta distribution. Irrespective of FF or FB mode of operation of atomizer, double overlapping Gaussian fits PDF of droplet size. Further, the separation of two Gaussian means changes with AFR and axial, radial locations indicates the change in probability distribution.
- In the case of FF mode of operation, SMD and MMD tend to increase initially due to coalescence of the spray and begin to decrease due to continued secondary breakup process. Existence of ligaments and flapping instability being dominant breakup process in FF mode of atomization explain faster decay of mean axial velocity compared to FB atomization. The JPDF of droplet size and axial velocity showed a long tail in the lower velocity range compared to that of FB. Also, a shift from unimodal to bimodal in the JPDF distribution is observed axially and radially, due to increased resistance of ambient air.

Compliance with Ethical Standards

Conflict of interest The authors declare that they have no conflict of interest.

References

Agrawal, S.R., Jiang, L., Agrawal, A.K., Midkiff, K.C.: High-speedvisualization of two-phase flow inside a transparent fuel injector. In: 8th U.S National Combustion Meeting held at University of Utah May 19-22, Paper ID: 070HE-0317 (2013). https://sutherland.che.utah.edu/USCI2013/PAPERS/2G12-070HE-0317.pdf

Ayres, D., Caldas, M., Semião, V., Da Graça Carvalho, M.: Prediction of the droplet size and velocity joint distribution for sprays. Fuel **80**(3), 383–394 (2001). https://doi.org/10.1016/S0016-2361(00)00094-6

Azevedo, C.G., Andrade, C.D., Costa, F.D.S.: Effects of nozzle exit geometry on spray characteristics of a blurry injector. Atomi. Sprays **23**(3), 193–209 (2013a). https://doi.org/10.1615/AtomizSpr.2013007244

Azevedo, C.G., de Andrade, J.C., Costa, F.D.S.: Experimental valuation diagnostics of hydrous ethanol sprays formed by a blurry injector. J. Aerosp. Technol. Manag. **5**(2), 197–204 (2013b). https://doi.org/10.5028/jatm.v5i2.231

Azevedo, C.G., de Andrade, J.C., Costa, F.S.: Effects of injector tip design on the spray characteristics of soy methyl ester biodiesel in a blurry injector. Renew Energy **85**, 287–294 (2016). https://doi.org/10.1016/j.renene.2015.06.021

Bhagwan, R., Habisreuther, P., Zarzalis, N., Turrini, F.: An experimental comparison of the emissions characteristics of standard jet A-1 and synthetic fuels. Flow Turbul. Combust. **92**(4), 865–884 (2014). https://doi.org/10.1007/s10494-014-9528-6

Biswal, A., Kale, R., Balusamy, S., Banerjee, R., Kolhe, P.: Lemon peel oil as an alternative fuel for GDI engines: a spray characterization perspective. Renew. Energy **142**, 249–263 (2019). https://doi.org/10.1016/j.renene.2019.04.087

Bottone, F., Kronenburg, A., Gosman, D., Marquis, A.: The numerical simulation of diesel spray combustion with LES-CMC. Flow Turbul. Combust. **89**(4), 651–673 (2012). https://doi.org/10.1007/s10494-012-9415-y

Carlton, M.A., Devore, J.L.: Probability with Applications in Engineering, Science, and Technology. Springer, Berlin (2017). https://doi.org/10.1007/978-3-319-52401-6

Chen, B., Gao, D., Liang, Y., Zhao, J., Sun, Y.: Experimental investigation of atomization and droplet turbulence characteristics of a twin-fluid nozzle with different self-excited vibrating cavity structures. Exp. Therm Fluid Sci. **99**, 525–536 (2018). https://doi.org/10.1016/j.expthermflusci.2018.08.017

Fisher, B.T., Weismiller, M.R., Tuttle, S.G., Hinnant, K.M.: Effects of fluid properties on spray characteristics of a flow-blurring atomizer. J. Eng. Gas Turbines Power **140**(4), 041511 (2017). https://doi.org/10.1115/1.4038084

Gad, H.M., Ibrahim, I.A., Abdel-baky, M.E., Abd El-samed, Farag, T.M.: Experimental study of diesel fuel atomization performance of air blast atomizer. Exp. Therm Fluid Sci. **99**, 211–218 (2018). https://doi.org/10.1016/j.expthermflusci.2018.07.006

Gañán-Calvo, A.M.: Enhanced liquid atomization: from flow-focusing to flow-blurring. Appl. Phys. Lett. **86**(21), 214101 (2005). https://doi.org/10.1063/1.1931057

Groom, S., Schaldach, G., Ulmer, M., Walzel, P., Berndt, H.: Adaptation of a new pneumatic nebulizer for sample introduction in ICP spectrometry. J. Anal. At. Spectrom. **20**(3), 169–175 (2005). https://doi.org/10.1039/B410772C

Jiang, L., Agrawal, A.K.: Investigation of glycerol atomization in the near-field of a flow-blurring injector using time-resolved PIV and high-speed visualization. Flow Turbul. Combust. **94**(2), 323–338 (2015a). https://doi.org/10.1007/s10494-014-9572-2

Jiang, L., Agrawal, A.K.: Spray features in the near field of a flow-blurring injector investigated by high-speed visualization and time-resolved PIV. Exp. Fluids (2015b). https://doi.org/10.1007/s00348-015-1973-z

Jiang, C., Parker, M.C., Spencer A., Wigley, G., Garner, C.P., Helie, J.: Droplet size development in a DISI injector fuel spray. In: Proc. 18th International Symposium on Applications of Laser and Imaging Techniques to Fluid Mechanics, Lisben, Portugal. July 4–7. (2016). http://ltces.dem.ist.utl.pt/lxlaser/lxlaser2016/finalworks2016/papers/01.14_2_195paper.pdf

Kasabov, P., Zarzalis, N., Habisreuther, P.: Experimental study on lifted flames operated with liquid kerosene at elevated pressure and stabilized by outer recirculation. Flow Turbul. Combust. **90**(3), 605–619 (2013). https://doi.org/10.1007/s10494-013-9444-1

Khan, M.A., Katoch, A., Gadgil, H., Kumar, S.: First step towards atomization at ultra-low flow rates using conventional twin-fluid atomizer. Exp. Therm Fluid Sci. **109**, 109844 (2019). https://doi.org/10.1016/j.expthermflusci.2019.109844

Kooij, S., Sijs, R., Denn, M.M., Villermaux, E., Bonn, D.: What determines the drop size in sprays? Phys Rev X **8**(3), 031019 (2018). https://doi.org/10.1103/PhysRevX.8.031019

Kooij, S.A., Moqaddam, A.M., de Goede, T.C., Derome, D., Carmeliet, J.: Sprays from droplets impacting a mesh. J. Fluid Mech. **871**, 489–509 (2019). https://doi.org/10.1017/jfm.2019.289

Kourmatzis, A., Lowe, A., Masri, A.: Combined effervescent and airblast atomization of a liquid jet. Exp. Therm Fluid Sci. **75**, 66–76 (2016). https://doi.org/10.1016/j.expthermflusci.2016.02.002

Kulkarni, A., Deshmukh, D.: spatial drop-sizing in airblast atomization: an experimental study. Atomization Sprays **27**(11), 949–961 (2017). https://doi.org/10.1615/AtomizSpr.2017021428

Lal, S., Kushari, A., Gupta, M., Kapoor, J.C., Maji, S.: Experimental study of an air assisted mist generator. Exp. Therm Fluid Sci. **34**(8), 1029–1035 (2010). https://doi.org/10.1016/j.expthermflusci.2010.03.006

Lefebvre, A.H.: Airblast atomization. Prog. Energy Combust. Sci. **6**(3), 233–261 (1980). https://doi.org/10.1016/0360-1285(80)90017-9

Lefebvre, A.H.: Atomization Sprays, 2nd (edn.). CRC Press, Boca Raton (1989). https://doi.org/10.1201/9781315120911

Liu, M., Duan, Y., Zhang, T.: Evaluation of effervescent atomizer internal design on the spray unsteadiness using a phase/Doppler particle analyzer. Exp. Therm Fluid Sci. **34**(6), 657–665 (2010). https://doi.org/10.1016/j.expthermflusci.2009.12.007

Lorenzetto, G.E., Lefebvre, A.H.: Measurements of drop size on a plain-jet airblast atomizer. AIAA J. **15**(7), 1006–1010 (1977). https://doi.org/10.2514/3.60742

Lujaji, F.C., Boateng, A.A., Schaffer, M., Mtui, P.L., Mkilaha, I.S.: Spray atomization of bio-oil/ethanol blends with externally mixed nozzles. Exp. Therm Fluid Sci. **71**, 146–153 (2016). https://doi.org/10.1016/j.expthermflusci.2015.10.020

Ma, X., Duan, Y., Liu, M.: Atomization of petroleum-coke sludge slurry using effervescent atomizer. Exp. Therm Fluid Sci. **46**, 131–138 (2013). https://doi.org/10.1016/j.expthermflusci.2012.12.003

Marmottant, P., Villermaux, E.: On spray formation. J. Fluid Mech. **498**, 73–111 (2004). https://doi.org/10.1017/S0022112003006529

Murugan, R., Bollu, B., Sekhar, K., Kolhe, P.S.: Experimental study of flow blurring twin fluid atomization concept using transparent injector. In: 14th Triennial International Conference on Liquid Atomization and Spray Systems, Chicago, IL, USA. July 22-26, Paper ID: 208, pp. 1–8 (2018). https://www.iclass2018.org/program/s208.html

Nukiyama, S., Tanasawa, Y.: Experiments on the Atomization of Liquids in an Air Stream- Reports 1 to 6. Tohoku Imperial University, Tech. rep. (Translated from the Transactions of the Society of Mechanical Engineers (Japan) v. 4, 5, and 6, 1938-40, by E. Hope. Publisher: Ottawa Defence Research Board, Dept. of National Defence (1950). (1938)

Ochowiak, M.: The experimental study on the viscosity effect on the discharge coefficient for effervescent atomizers. Exp. Therm Fluid Sci. **50**, 187–192 (2013). https://doi.org/10.1016/j.expthermflusci.2013.06.008

Ochowiak, M.: Discharge coefficient of effervescent atomizers with the swirl motion phenomenon. Exp. Therm Fluid Sci. **79**, 44–51 (2016). https://doi.org/10.1016/j.expthermflusci.2016.06.026

Ochowiak, M., Broniarz-Press, L., Rozanski, J.: The discharge coefficient of effervescent atomizers. Exp. Therm Fluid Sci. **34**(8), 1316–1323 (2010). https://doi.org/10.1016/j.expthermflusci.2010.06.003

Panchasara, H.V., Agrawal, A.K.: Characteristics of preheated bio-oil sprays produced by an air-blast injector. In Proceedings of ASME Turbo Expo 2010: Power for Land, Sea and Air, Gaksgow UK, June 14–18, GT2010-23397, pp. 619–629 (2010). https://doi.org/10.1115/GT2010-23397

Panchasara, H.V., Kolhe, P.S., Agrawal, A.K.: Spray flame characteristics of bio-derived fuels in a simulated gas turbine burner. In: Proceedings of ASME Turbo Expo 2019: Power for Land, Sea and Air, GT2019-90663, pp. 1–10. (2019). https://doi.org/10.1115/GT2019-90663

Panchasara, H.V., Simmons, B.M., Agrawal, A.K., Spear, S.K., Daly, D.T.: Combustion performance of biodiesel and diesel-vegetable oil blends in a simulated gas turbine burner. J. Eng. Gas Turbines Power **131**(3), 031503 (2009). https://doi.org/10.1115/1.2982137

Raju, M., Saravanan, B., Kolhe, P.S.: Experimental investigation of the spray spatial structure of novel flow blurring twin-fluid atomizer. In 14th Triennial International Conference on Liquid Atomization and Spray Systems, Chicago, IL, USA. July 22-26, Paper ID: 220, pp. 1–8. (2018) https://www.iclass2018.org/program/s220.html

Simmons, B.M., Agrawal, A.K.: Flow blurring atomization for low-emission combustion of liquid biofuels. Combust. Sci. Technol. **184**(5), 660–675 (2012). https://doi.org/10.1080/00102202.2012.660222

Simmons, B.M., Panchasara, H.V., Agrawal, A.K.: A comparison of air-blast and flow-blurring injectors using phase Doppler particle analyzer technique. In: Proceedings of ASME Turbo 2009: Power for Land, Sea and Air—GT2009-60239, pp. 981–992 (2009). https://doi.org/10.1115/GT2009-60239

Soni, S.K., Kirar, P.K., Kolhe, P.S., Sahu, K.C.: Deformation and breakup of droplets in an oblique continuous air stream. Int. J. Multiphase Flow **122**, 103141 (2020). https://doi.org/10.1016/j.ijmultiphaseflow.2019.103141

Sovani, S.D., Sojka, P.E., Lefebvre, A.H.: Effervescent atomization. Prog. Energy Combust. Sci. **27**(4), 483–521 (2001). https://doi.org/10.1016/S0360-1285(00)00029-0

Stiehl, R., Schorr, J., Krüger, C., Dreizler, A., Böhm, B.: In-cylinder flow and fuel spray interactions in a stratified spray-guided gasoline engine investigated by high-speed laser imaging techniques. Flow Turbul. Combust. **91**(3), 431–450 (2013). https://doi.org/10.1007/s10494-013-9500-x

Sun, C., Ning, Z., Qiao, X., Lv, M., Li, Y., Zhao, J., Wang, X.: Measurements of internal flow regime and bubble size in effervescent atomizer. Exp. Therm Fluid Sci. **98**, 604–620 (2018). https://doi.org/10.1016/j.expthermflusci.2018.07.002

Wright, Y.M., Margari, O.N., Boulouchos, K., De Paola, G., Mastorakos, E.: Experiments and simulations of *n*-heptane spray auto-ignition in a closed combustion chamber at diesel engine conditions. Flow Turbul. Combust. **84**(1), 49–78 (2010). https://doi.org/10.1007/s10494-009-9224-0